Rotor Electrical Fault Detection in DFIGs Using Wide-Band Controller Signals

Nur Sarma, *Member, IEEE*, Paul M. Tuohy, Anees Mohammed, and Siniša Djurović, *Member, IEEE*

***Abstract*—This paper presents a novel study of the wide-band spectral signatures in the controller signals of doubly fed induction generators (DFIGs) for the identification of rotor electrical faults. The aim is to advance the understanding of diagnostic information obtainable from the readily available DFIG controller signals. Analytical equations defining the controller signals possible spectral contents are derived to enable characterization of spectral signatures and their correlation to operating conditions and rotor faults. The equations are verified in a DFIG harmonic model study and also validated by undertaking a range of experiments on a laboratory DFIG test-rig. It is shown that the calculated, simulated and experimental results are in good agreement with regards to representing fault induced signatures in the examined DFIG controller signals spectra. Furthermore, it is shown that wide-band rotor electrical fault related spectral signatures in the controller signals carry considerable diagnostic potential for recognition of rotor electrical faults.**

***Index Terms*—Condition monitoring, doubly fed induction generator, harmonic machine model, rotor electrical fault, signature analysis, Simulink, wind turbine.**

I. Introduction

WIND power is becoming an important contributor to global electricity generation, which is expected to reach 2000 GW of installed capacity by 2030 [1]. Reducing the cost of wind electricity generation would be a significant benefit, which can be achieved by reducing the currently significant operations & maintenance (O&M) costs. O&M costs of a wind turbine (WT) are around 10-25% of the total cost of the electricity [2]. Effective condition monitoring (CM) and fault detection techniques, therefore, could considerably contribute to cost reductions by identifying potential impending faults in WT components.

WT failures have been studied in [3]–[5], which identified that the generator generally causes the highest annual downtime per year. Furthermore, the generator is also reported to be the greatest contributor to major offshore WT repairs and typically has high repair costs [6]. Understanding generator faults and developing effective non-invasive low cost methods for reliable fault detection, therefore, remains of considerable interest.

The doubly fed induction generator (DFIG) topology is a widely used generator topology (Type 3) in the currently installed MW size WTs due to its technical advantages [7], [8]. Consequently, fault detection methods for DFIG WTs have received significant attention in the literature [2], [9]–[11].

This paper presents a novel study that investigates the effects of rotor electrical faults on the wide-band controller signals spectra of DFIGs for potential fault detection purposes. Multiple signals including vibration, torque, temperature and SCADA signals have been previously investigated for WT generator fault detection [12], [13]. However, monitoring of these signals invariably imposes a relatively significant additional cost to CM and fault detection systems due to the requirements for dedicated sensing and specialized data conditioning and acquisition devices [12].

As an alternative, utilizing the readily available generator electrical signals for fault detection has been previously explored, as these have been shown to contain fault specific changes [4], [14], [15]. Electrical signals based fault detection techniques generally utilize the easily accessible generator terminal signals such as the stator currents, which impose somewhat reduced sensing requirements [12]. In addition to requiring dedicated sensing, these electrical signals may not be sufficient for effective fault detection, as a generator is controlled through a closed-loop control system, which can act to suppress the fault related spectral signatures in the terminal signals [16]. Exploration of methods that utilize fault detection information embedded within the readily available DFIG controller signals has therefore started to receive attention [17]–[19]. Fault detection techniques that use the controller signals can in theory provide a number of attractive advantages, as they require no installation of additional sensors or data acquisition devices. Furthermore, they minimize the masking effect of the controllers to fault related changes that can be pronounced in the terminal signals [9], [11], [19].

The utilization of different controller signals for fault detection purposes have been previously reported for conventional and DFIG drives including: *dq*-axis rotor currents for stator and rotor asymmetries [16], [20]; error signals of the *dq*-axis rotor currents for rotor electrical asymmetry [9]; rotor modulating signals for stator and rotor asymmetries [11]; rotor voltage for

Manuscript received August 16, 2019; revised February 28, 2020; accepted June 11, 2020. Date of publication August 5, 2020; date of current version December 16, 2020. This work was supported by the UK Engineering and Physical Sciences Research Council HOME-Offshore: Holistic Operation and Maintenance for Energy from Offshore Wind Farms Consortium under Grant EP/P009743/1. *(Corresponding author: Nur Sarma.)*

Nur Sarma is with the Electrical and Electronic Engineering Department, Duzce University, Duzce 81620, Turkey (e-mail: nursarma@duzce.edu.tr).

Paul M. Tuohy, Anees Mohammed, and Siniša Djurović are with the University of Manchester, Manchester M13 9PL, U.K. (e-mail: paul.tuohy-2@manchester.ac.uk; anees.mohammed@manchester.ac.uk; sinisa.durovic@manchester.ac.uk).

Color versions of one or more of the figures in this article are available online at https://ieeexplore.ieee.org.

Digital Object Identifier 10.1109/TSTE.2020.3014446

stator and rotor electrical asymmetry [21]; and, stator reactive power for inter-turn short circuit faults and eccentricity faults [10], [22]. However, these studies largely focused on examining only the fundamental harmonic related spectral signatures of the controller signals and did not assess the wide-band, higher order, fault related spectral signatures that could, in principle, carry significant fault detection potential [23]–[25].

The focus of this work, therefore, is the investigation of these effects, which could provide a better understanding of the capability of the controller signals being used for identification of generator faults. Rotor electrical faults, which generally manifest through rotor electrical asymmetry (REA), are of particular interest, as these have been shown to significantly impact WT generator total failure rates for all sizes of WTs [9], [26], [27].

This paper investigates DFIG controller signals wide-band spectra with a view to characterizing their fault related spectral signatures and assessing the possibility of their utilization for REA fault detection. An electromagnetic origin analytical study of the wide-band spectral signatures of the controller signals with and without REA is first performed, which yields equations that define fault related spectral signatures and relates them to operating conditions and generator design features (e.g. slip, supply frequency, pole-pair number, etc.).

A DFIG harmonic model, which is capable of representing electrical fault effects, is then used to characterize the wide-band REA related spectral signatures in the terminal and controller signals of DFIGs, and to verify the presented analytical equations. Experimental investigations are subsequently conducted on a purpose built laboratory DFIG test-rig to validate the presented equations and simulation results. Lastly, the fault detection potential of the identified wide-band REA related spectral signatures of the controller signals are also experimentally investigated.

II. Controller Signals Spectral Content With REA

This section defines the equations for calculation of the possible spectral content of a DFIG's controller signals for operation with and without REA. It is assumed that a healthy DFIG system is electrically balanced; that the higher order supply harmonics and associated spectral effects are ignored; and, that the system is controlled with a conventional stator flux oriented control (SFOC) scheme for the purposes of this study [28]–[30].

A. Healthy Operating Condition

During healthy operation (balanced supply and windings), a number of interharmonic frequency components can appear in the spectra of the terminal signals. These frequency components (referred to as 'carrier frequencies' in further text) are caused by the air-gap harmonic field distribution and are related to multiple factors including operating speed, supply frequency, supply harmonic order and air-gap magnetic field pole-pair number, etc., [23], [30], [31].

The possible carrier frequencies in the stator, $\mathrm{f_{Is}^{H}}$, and rotor, $\mathrm{f_{Ir}^{H}}$, currents are [23], [31]:

$$f_{Is}^{H} = |1 \pm 6k\,(1-s)|\,f_s \tag{1}$$

$$f_{Ir}^{H} = |s \pm 6k\,(1-s)|\,f_s, \tag{2}$$

where: k is related to the air-gap magnetic field pole number ($k = 0, 1, 2, \ldots$); s is the slip; and, f_s and sf_s are the fundamental frequencies of the stator and rotor currents, respectively.

The carrier frequencies in the terminal signals will map into counterpart carrier frequencies in the controller signals. These can be defined analytically by converting (1) and (2) from their natural stator and rotor reference frames, respectively, to the synchronously rotating stator flux oriented reference frame by applying the standard Park transformation, to give the following equation to calculate the possible carrier frequencies, $\mathrm{f_{C}^{H}}$, in the controller signals [28]:

$$f_{C}^{H} = |6k\,(1-s)|\,f_s. \tag{3}$$

In addition, it can be shown that the three-phase stator currents and voltages are used to calculate the stator active and reactive power signals whose carrier frequencies are also defined by (3) [24], [28].

B. Rotor Electrical Asymmetry Operating Condition

The existence of REA is characteristic of a rotor electrical fault(s). If a rotor fault and thus, REA occurs, $\pm 2sf_s$ sideband frequencies arise around the stator currents carrier frequencies (defined by (1)), to yield the following possible REA related sideband frequencies in the stator currents [31], [32]:

$$f_{Is}^{REA} = |(1 \pm 2s) \pm 6k\,(1-s)|\,f_s. \tag{4}$$

Again, the stator active and reactive power signals are calculated using the three-phase stator currents and voltages (see Appendix A), to produce the spectral contents with REA, which can be defined as:

$$f_{C}^{REA} = |2s \pm 6k\,(1-s)|\,f_s. \tag{5}$$

The rotor currents spectral content with REA, however, do not exhibit a significant difference compared to that existing in a healthy machine [31]. REA will not produce new distinct REA related frequency components in the rotor reference frame but will, however, give rise to reverse sequence frequency components at the frequencies existing in the spectra of the healthy rotor currents [31], as defined by (6).

$$f_{Ir}^{REA} = \mp |s \mp 6k\,(1-s)|\,f_s. \tag{6}$$

The transformation of the spectral content of the faulty rotor currents to the synchronously rotating stator flux oriented reference frame produces new frequency components displaced by $\pm 2sf_s$ from the frequency components calculated by (3), and can be defined by (5) (see Appendix B).

The expressions to calculate the possible frequency components in the controller signals of DFIGs are summarized in Table I, and the spectral contents are illustrated in Fig. 1. In Fig. 1, Ps$*$ and Qs$*$ are the reference stator active and reactive powers, respectively; Ps and Qs are the stator active and reactive powers, respectively; ePs and eQs are the stator active and reactive power error signals, respectively; Ird$*$ and Irq$*$ are the reference d- and q-axis rotor currents, respectively; Ird and Irq are the d- and q-axis rotor currents, respectively; eIrd and eIrq

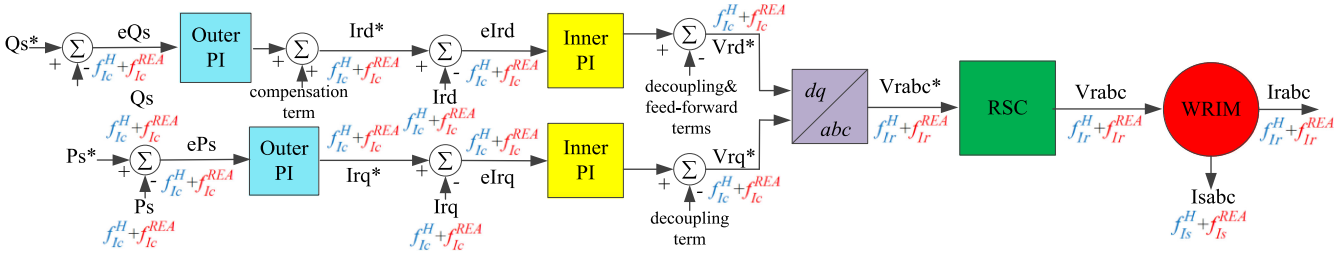

Fig. 1. Frequency components distribution of the SFOC scheme in the DFIG operating without (blue terms only) and with REA (blue and red terms).

TABLE I
SPECTRAL CONTENT OF THE CONTROLLER SIGNALS

Healthy Operating Condition	*REA Operating Condition*
$\|6k(1\text{-}s)\|f_s$	$\|2s \pm 6k(1\text{-}s)\|f_s$ $\| 6k(1\text{-}s)\|f_s$

are the d- and q-axis rotor current error signals, respectively; Vrd$*$ and Vrq$*$ are the reference d- and q-axis rotor voltages, respectively; Vrabc$*$ are the reference three-phase rotor voltages; Vrabc and Irabc are the three-phase rotor voltages and currents, respectively; and, Isabc are the three-phase stator currents.

Fig. 1 illustrates that the d- and q-axis controller signals have the same the spectral contents. This is caused by the origins of these signals, as well as the assumption that identical tuning procedures were implemented on the dq-axis controllers [29].

Fig. 1 represents the frequency contents of the electrical signals from a DFIG with the implementation of a SFOC scheme. It shows that the frequency contents of the electrical signals vary with the implementation of an unbalanced rotor (*blue*: the frequency contents of the electrical signals for healthy operating condition; and, *blue+red*: the frequency contents of the electrical signals for a REA operating condition). The frequency content illustrated in Fig. 1 enables creating a frequency map, which can be used to understand the nature of REA signatures and thus, to develop real-time frequency monitoring and tracking condition monitoring schemes. These schemes can observe fault associated magnitudes and hence, can help to make diagnostic decisions.

III. REA Analysis Using DFIG Harmonic Model

To understand the effects of REA on the wide-band spectra of the controller signals, a time-stepped SFOC controlled DFIG harmonic model was developed in Matlab SIMULINK. The DFIG harmonic model is capable of representing arbitrary electrical asymmetries and their spectral signatures, and is based on the principles presented in [28]. The DFIG harmonic model consists of a wound rotor induction machine (WRIM) harmonic model coupled to a SFOC model, and uses as data inputs the design and operational information of the DFIG laboratory test-rig used in this work (specified in Section IV). The WRIM harmonic model uses the Conductor Distribution Function approach to calculate harmonic inductance values [31], [33] and is able to represent higher order air-gap magnetic field effects in the spectra of the terminal signals and thus, the controller signals.

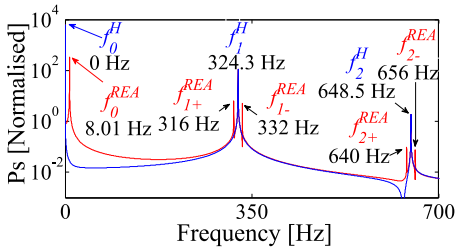

Fig. 2. FFT spectrum of Ps.

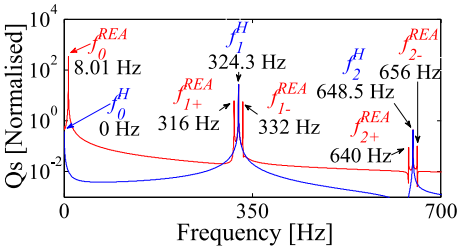

Fig. 3. FFT spectrum of Qs.

For the sake of brevity, the simulation results for a typical steady-state operating point in the super-synchronous region (Ps$* = -6.5$ kW and Qs$* = 0$ Var at 1,620 rpm) are presented in this section. (It is to be noted that consistent results were obtained for other typical operating points in both the sub- and super-synchronous operating regions.)

For the purposes of this study, supply unbalance and speed ripple effects were not incorporated into the calculations. REA was modeled by implementing an additional resistance in series with one phase of the WRIM [34]. To clearly illustrate the effects of REA, one phase resistance was increased by 320% [9]. The controller signals spectra were investigated in a 0–700 Hz bandwidth, since REA related frequency components generally weaken in magnitude at higher frequencies [24].

The predicted controller signals spectra with REA (red line) and without REA (blue line) are presented in Figs. 2–13. The carrier frequencies (calculated using (1)-(3)), and REA related sideband frequencies (calculated using (4)-(6)) are labeled in the figures for clarity. The values of the parameter k ($k = 0$, 1 and 2) are labeled in the figures using the subscripts '0', '1' and '2', whilst the '-' and '+' denote the position of the specific REA related sideband frequencies with respect to their carrier frequencies (e.g. '-' considers $[2s - 6k(1-s)f_s]$ in (5)).

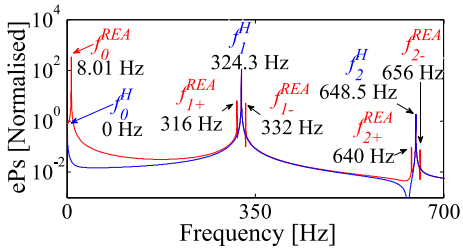

Fig. 4. FFT spectrum of ePs.

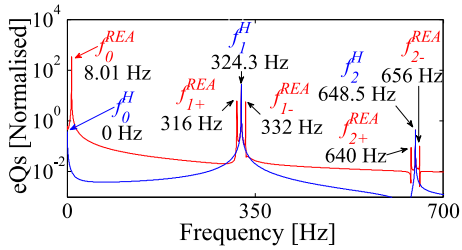

Fig. 5. FFT spectrum of eQs.

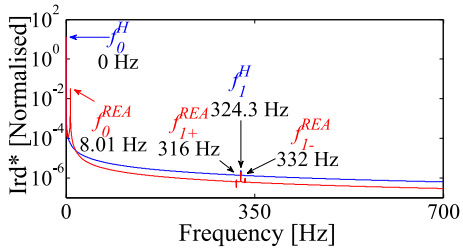

Fig. 6. FFT spectrum of Ird∗.

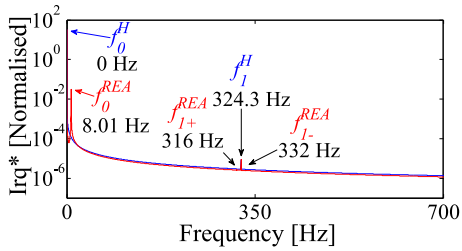

Fig. 7. FFT spectrum of Irq∗.

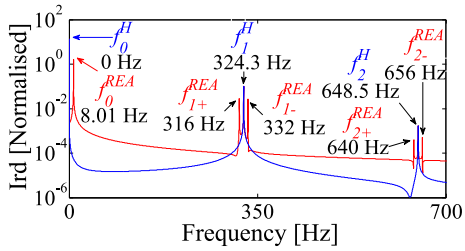

Fig. 8. FFT spectrum of Ird.

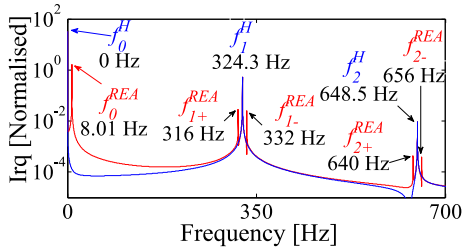

Fig. 9. FFT spectrum of Irq.

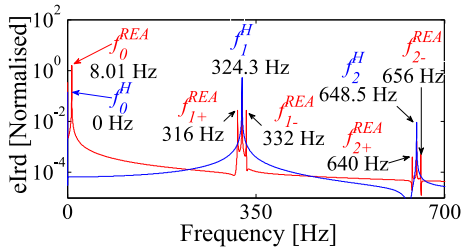

Fig. 10. FFT spectrum of eIrd.

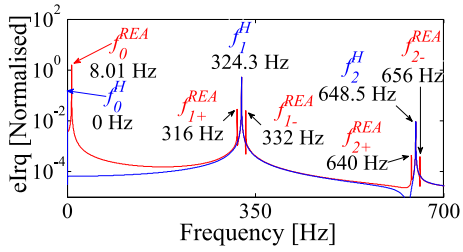

Fig. 11. FFT spectrum of eIrq.

The results presented in Figs. 2–13 are seen to verify the equations used to calculate the wide-band REA related frequency components in the controller signals (calculated using (5)). The calculated frequency components for healthy and REA operating conditions are presented in Table II.

Figs. 2–13 show that, as expected, the carrier frequencies are present in both the healthy and REA spectra of the controller signals. However, the REA related sideband frequencies, acting as fault signatures, arise in the spectra of the controller signals during the REA operating condition. The REA related sideband frequencies manifest as $\pm 2sf_s$ sidebands on all carrier frequencies present in the healthy controller signals. The DFIG harmonic model results illustrate that REA related sideband frequencies are prominent in both the spectra of the outer and inner control loops signals with the exception of Ird∗ and Irq∗. This is because, as expected, the outer controllers act as low-pass filters and suppress the magnitudes of the wide-band frequency components in Ird∗ and Irq∗.

IV. Experimental Test-Rig

A 30 kW laboratory DFIG test-rig was used for experimental investigations. The test-rig contains a 415 V, four-pole, three-phase, 50 Hz, WRIM coupled to a DC machine (acting as a prime mover). The DC machine is set to operate at a desired predefined constant speed during experiments via a commercial CT MENTOR-II-M75R DC drive unit. The stator windings of the WRIM are connected to the grid whereas its rotor windings

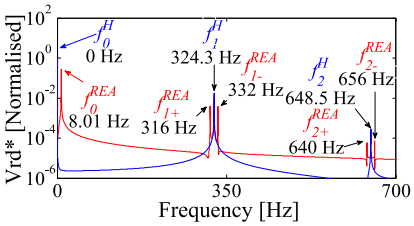

Fig. 12. FFT spectrum of Vrd∗.

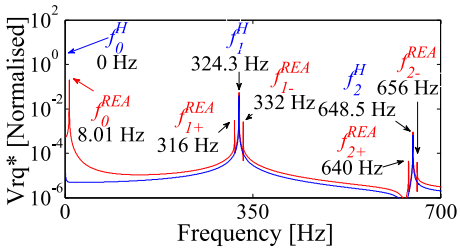

Fig. 13. FFT spectrum of Vrq∗.

TABLE II
CALCULATED FREQUENCY COMPONENTS OF THE CONTROLLER SIGNALS FOR 1620 RPM

k	Healthy [Hz], eq. (3)	REA [Hz], eq. (5)	
0	$f_0^H = 0$	$f_0^{REA} = 8$	
1	$f_1^H = 324$	$f_{1+}^{REA} = 316$	$f_{1-}^{REA} = 332$
2	$f_2^H = 648$	$f_{2+}^{REA} = 640$	$f_{2-}^{REA} = 656$

are connected to an industrial back-to-back converter (comprising two CT UNIDRIVE SP-4401 units) coupled with a DC link: a grid side (GSC) and a rotor side converter (RSC). A SFOC scheme was implemented on the RSC using a dedicated real-time routine executed on a dSPACE platform and a resolver communications module [29], [35]. This enabled access to the controller signals of interest whilst retaining the use of the commercial converters.

The stator and rotor currents were measured using LEM LA 55-P sensors and the stator voltages using LEM LV25-600 transducers. The stator active and reactive powers were calculated in the dSPACE platform from the measured stator currents and voltages. Furthermore, the dSPACE platform was used for recording the DFIG terminal and controller signals examined in this study. The controller signals were subsequently imported into MATLAB in order to conduct FFT analysis. A post processing routine was implemented on the recorded time domain signals with a rectangular window 2^{19} point FFT routine in a bandwidth of 0–700 Hz, giving a resolution of ∼0.1 Hz. A 1024 ppr incremental encoder was used for rotor position measurements. Further details, as well as a full list of the parameters of the DFIG test-rig, can be found in [29], [35]. Fig. 14 illustrates the schematic diagram of the laboratory DFIG test-rig.

V. EXPERIMENTAL STUDY

This section presents an experimental study of the wide-band spectra of the controller signals from the laboratory DFIG

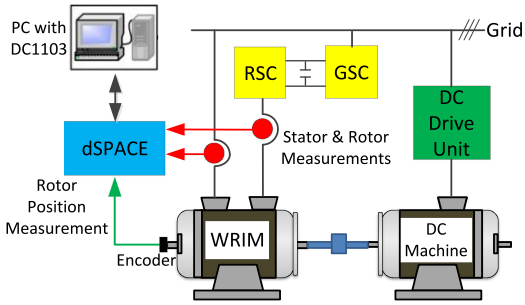

Fig. 14. Schematic diagram of the laboratory DFIG test-rig.

test-rig. The presented results are used to validate the analytical equations and the DFIG harmonic model predictions. The test-rig was operated with an active power demand of Ps∗ = -6.5 kW and a reactive power demand of Qs∗ = 0 VAr, as an arbitrary but representative operating point during the experiments [34].

For clarity, the experimental study is presented in two subsections: the measured spectra of the controller signals are reported in Subsection A, whilst the fault detection capability of the identified wide-band REA related frequency components is presented in Subsection B.

A. REA Signature Study

A fault level of 320% single phase rotor resistive unbalance and an operating speed of 1,620 rpm were chosen to be consistent with the DFIG harmonic model results presented in Section III. The spectral contents of the measured controller signals with and without REA are shown in Figs. 15–26. All the results in this subsection are normalized with respect to the DC component to enable direct comparison of all the wide-band spectral signatures. The previously calculated frequency components listed in Table II are labeled in Figs. 15–26 using the same nomenclature for consistency.

The experimental results show that the magnitudes of the REA related sideband frequencies (calculated by (5)) significantly increase when the DFIG operates with REA (Figs. 15–26.b –18) in comparison to those measured during healthy operation (Figs. 15–26.a). The frequencies of the measured REA related sideband are at practically the same values presented in Table II, confirming the analytical expressions (in Table I) and the validity of the predictions from the DFIG harmonic model. The slight differences between the calculated and experimental results are typically be caused by inherent minor variations in the grid frequency and operating speed during the tests.

As expected, the experimental results are noisier than the DFIG harmonic model results presented in Figs. 2–13. Furthermore, they also have additional frequency components, which largely arise from secondary effects such as grid supply harmonics; the inherent stator and rotor windings unbalance; speed ripple; and, switching harmonics, etc., [30], [32]. A number of these additional frequency components and their origins were identified in previous work [28] but to keep the figures relatively uncluttered in this paper, they are not labelled here, since they are beyond the scope of this study.

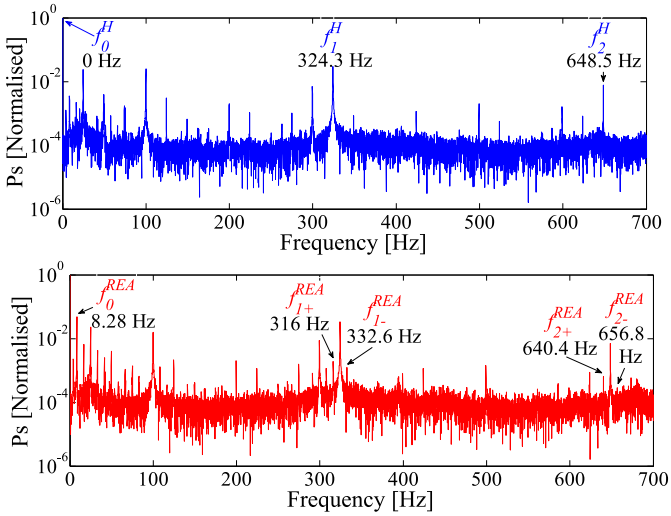

Fig. 15. Ps spectrum: healthy (top), and REA (bottom) operating condition.

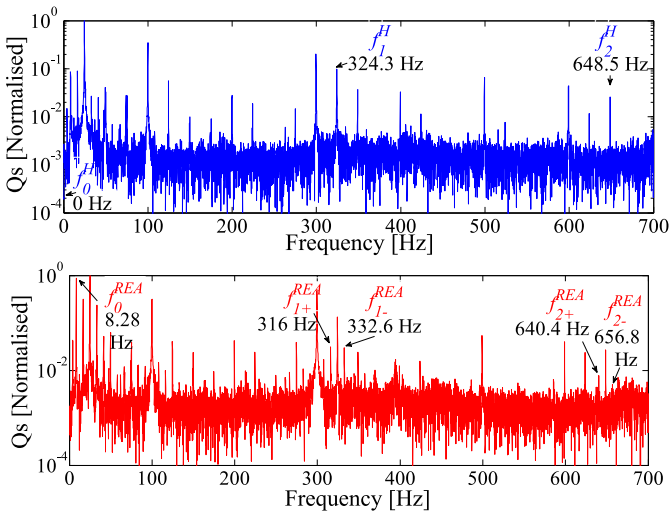

Fig. 16. Qs spectrum: healthy (top), and REA (bottom) operating condition.

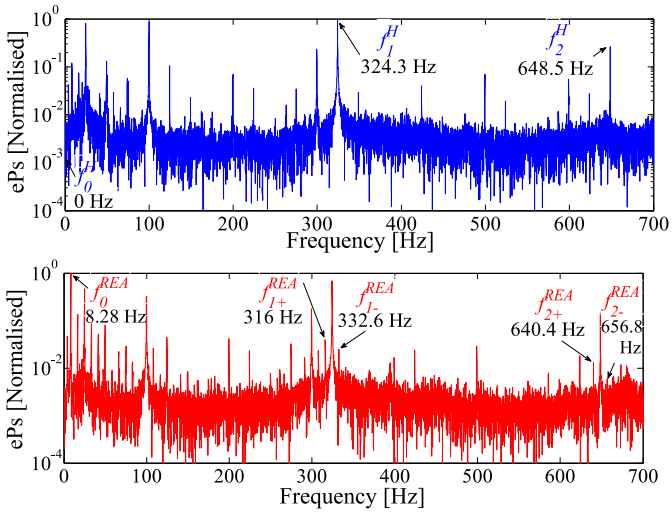

Fig. 17. ePs spectrum: healthy (top), and REA (bottom) operating condition.

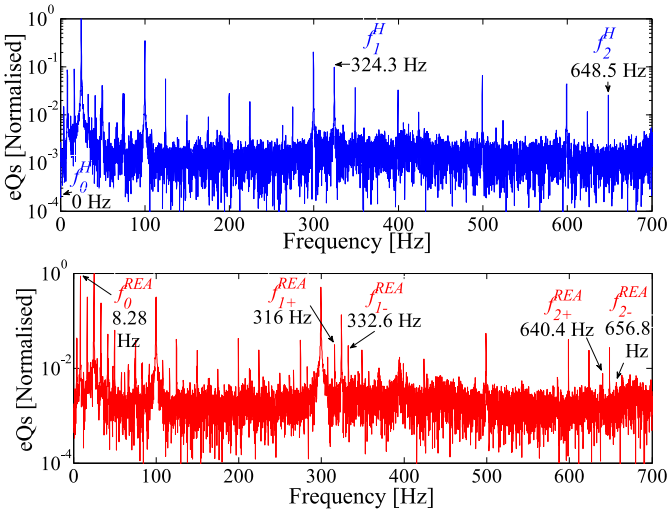

Fig. 18. eQs spectrum: healthy (top), and REA (bottom) operating condition.

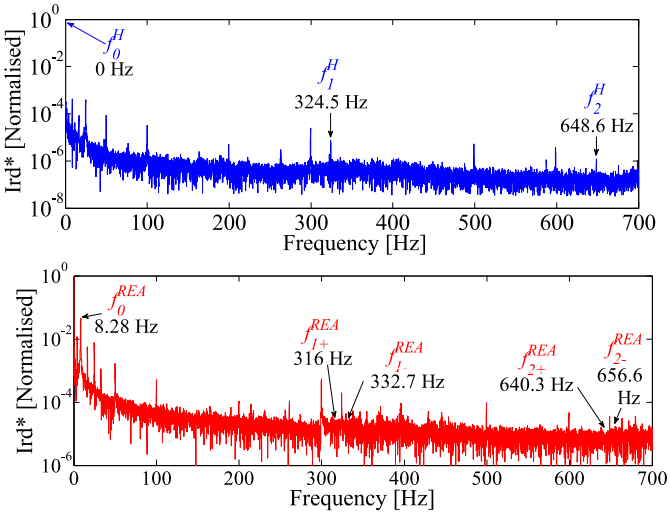

Fig. 19. Ird∗ spectrum: healthy (top), and REA (bottom) operating condition.

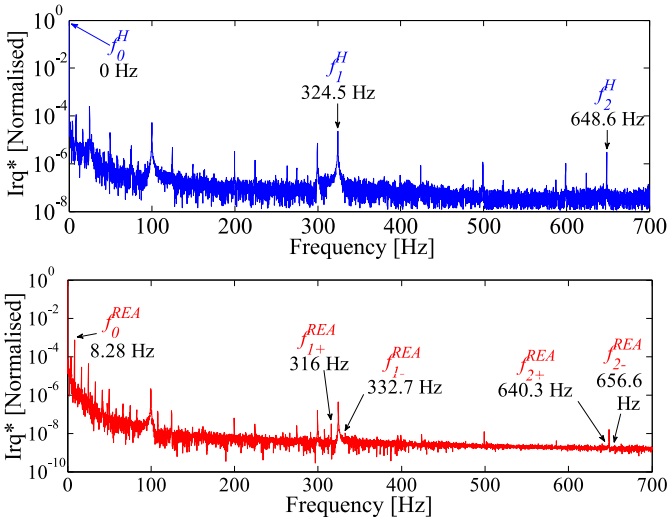

Fig. 20. Irq∗ spectrum: healthy (top), and REA (bottom) operating condition.

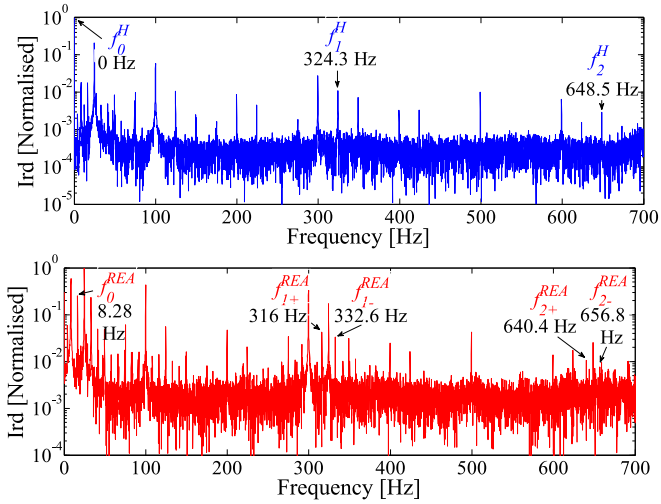

Fig. 21. Ird spectrum: healthy (top), and REA (bottom) operating condition.

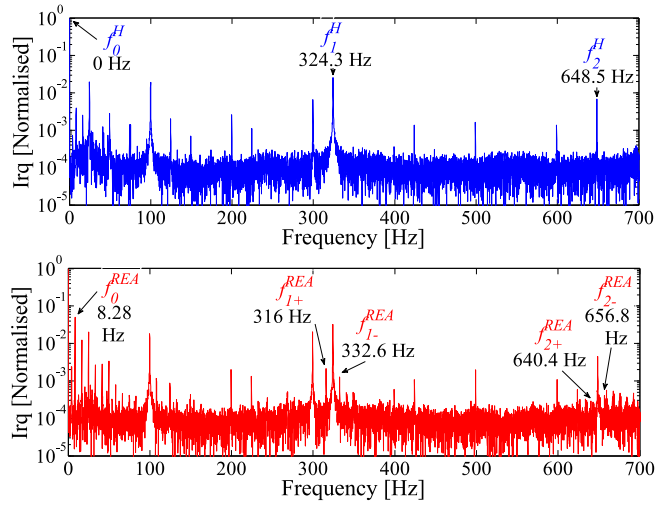

Fig. 22. Irq spectrum: healthy (top), and REA (bottom) operating condition.

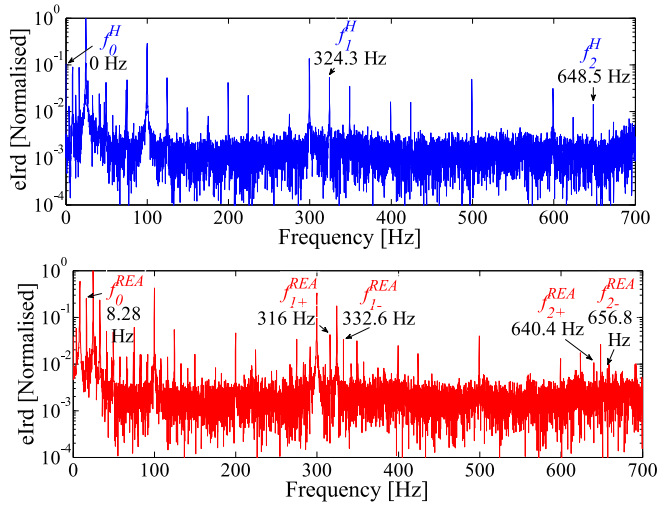

Fig. 23. eIrd spectrum: healthy (top), and REA (bottom) operating condition.

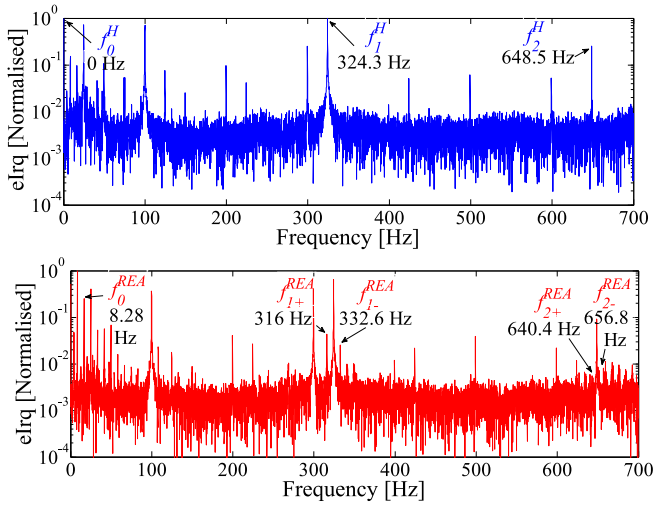

Fig. 24. eIrq spectrum: healthy (top), and REA (bottom) operating condition.

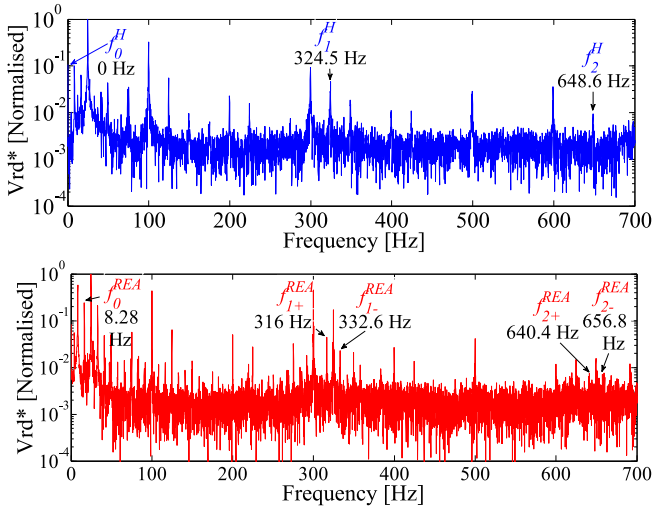

Fig. 25. Vrd∗ spectrum: healthy (top), and REA (bottom) operating condition.

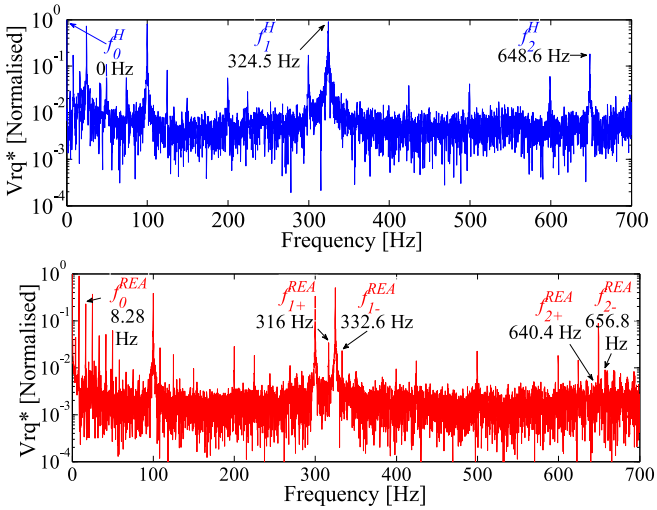

Fig. 26. Vrq∗ spectrum: healthy (top), and REA (bottom) operating condition.

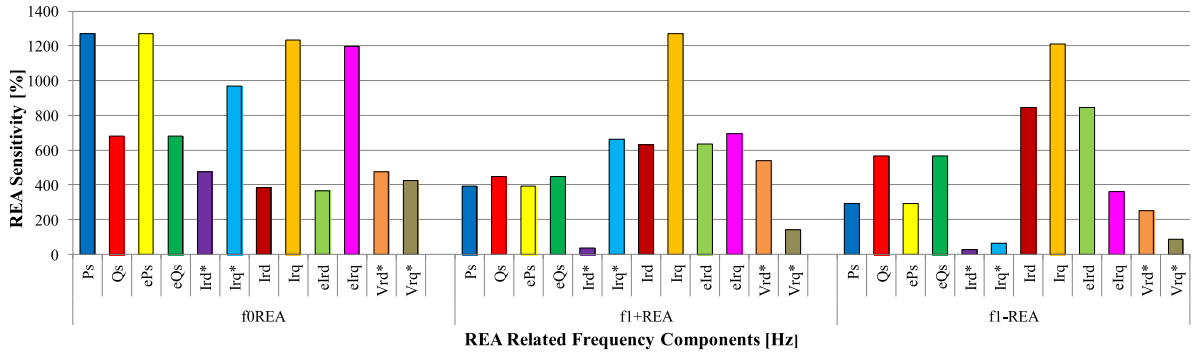

Fig. 27. Sensitivity study results for the REA related frequency components for 1,620 rpm.

Figs. 15–26.b show that, as is generally expected, the most prominent REA related sideband frequency is f_0^{REA}, which has been previously explored for fault detection purposes [9], [18]. However, the presented results clearly illustrate that higher order REA related sideband frequencies, f_k^{REA}, are also present in the spectra of the controller signals. For example, f_1^{REA} remains identifiable in all the examined controller signals spectra and would hence, have considerable potential as an REA indicator in addition to f_0^{REA}.

The magnitudes of the REA related sideband frequencies generally decrease at higher frequency levels, as is expected Furthermore, f_2^{REA} are potentially difficult to distinguish in several of the controller signals such as Irq (Fig. 22), since REA related sideband frequencies can disappear in the noise level. However, f_2^{REA} are generally obvious in Ird (Fig. 21). These results suggest that reliable identification of f_2^{REA} in the controller signals can be signal type dependent.

Further examination of the data presented in Figs. 15–26 shows that the controller signals with the highest REA detection potential (on the examined test system) are the outer controller loops signals Ps, ePs, Qs and eQs. All the wide-band REA related frequency components are clearly distinguishable in the spectra of these signals, as seen in Figs. 15.

B. REA Detection Sensitivity Study

To examine the fault detection potential of the identified wide-band REA related frequency components in the controller signals, a sensitivity study was performed. A sensitivity index was used to enable comparison of the REA detection potential of individual REA related frequency components. The sensitivity index is calculated as [26]:

$$\text{Sensitivity } [\%] = \frac{M^{REA} - M^{H}}{M^{H}} \times 100, \tag{7}$$

where: M^{REA} and M^{H} are the magnitudes of a specific REA related frequency components measured for healthy and REA conditions, respectively. f_0^{REA} and f_1^{REA} showed the most consistent fault detection potential in all the controller signals in the previous subsection and were therefore evaluated using (7). The previously presented experimental data for healthy, as well as 320% REA, was used to calculate the REA sensitivity of the REA related frequency components in the controller signals, and the results are presented in Fig. 27. Fig. 27 shows that the magnitudes of REA sensitivity can vary considerably for each controller signal and frequency component. Therefore, careful selection is paramount for accurate fault detection. For example, it can be seen that the REA sensitivity of f_0^{REA}, has the most prominent REA related frequency components, i.e. Ps, ePs, Irq∗, Irq and eIrq, which are all above 900% REA sensitivity. In addition, most of the controller signals wide-band REA related frequency components, f_{1+}^{REA} and f_{1-}^{REA}, have good sensitivity, and some signals, in fact, have higher REA sensitivity than f_0^{REA}. For example, f_{1+}^{REA} and f_{1-}^{REA} for Ird and eIrd are more sensitive than that of f_0^{REA}.

Fig. 27 also shows that the REA sensitivity of Irq consistently has the highest magnitude in comparison to the other controller signals across all the measured REA related sideband frequencies. As a result, the presented REA sensitivity study indicates that f_{1+}^{REA} and f_{1-}^{REA} have excellent REA detection capability, as they are extremely sensitive to REA, which was found to be a challenge for purely f_0^{REA} signals.

The identified high REA sensitivity of the f_{1+}^{REA} and f_{1-}^{REA} frequency components for most of the controller signals suggests that the wide-band REA related frequency components carry additional important and confirmatory REA fault detection potential.

VI. Discussion

The proposed condition monitoring and fault detection technique is non-invasive and there is minimal additional cost and complexity required to implement it. It has been applied to the DFIG experimental test-rig discussed in Section IV and has also been described in greater detail in [29]. The test-rig is a small-scale replica of a real WT system and the converters used in the test-rig are standard commercial converters, which are used in various industrial applications. The presented work has illustrated and validated how the proposed technique could be implemented in practical applications. However, if the proposed technique is to be used in real applications especially WT applications, the controller signals that are used as fault indicators will need to be sampled at a higher sampling frequency rate than what is typically implemented in present systems, i.e. in the order of several times a second verses several times an hour, as it now typically used. This is fairly simple to achieve and

would enable the application of transformation algorithms such as FFTs and any other transformation methods. The resolution of the sampled signals can normally be increased easily using the already installed measurement sensors without any requirement of additional devices.

The proposed condition monitoring and fault detection technique is capable of being utilized in other electrical drive systems that contain electric machines such as in electric vehicles, etc., as these drive systems also contains electric machines and controller units. The implementation of this technique could lead to potential benefits in terms of safety for drivers, passengers, other road users/vehicles, etc. Furthermore, it could help to maximize the life of products such as electric machines or gearboxes, as damage to these components would require an expensive overhaul and downtime for a vehicle and its associated driver. Therefore, the sampling of controller signals and then using them for condition monitoring and fault detection purposes is feasible and the benefits are potentially significant.

The main application for this investigated technique, however, and the main focus of the presented research was for WT applications, especially offshore WTs, since downtime of an offshore WT can be much more costly due to multiple factors including requiring shipping or helicopters to access an off-line WT due to a fault; specialist personnel; and, weather factors, etc. Therefore, to attend and repair a faulty WT increases the associated costs significantly compared to onshore wind turbines due to these factors.

The presented results in Fig. 27 show that the wide-band controller signals frequencies have good potential to be used for REA detection, as most of the controller signals wide-band REA related frequency components have high sensitivity, and in fact some of them (such as the inner control loop signals - Ird & Irq) are more sensitive to detect REA than the side band frequencies. Furthermore, data fusion methods to diagnostic techniques are receiving more research attention [32], since adoption of a data fusion approach that is dependent on the comparison of independent REA related signatures can be valuable in reducing false alarms, which may be caused by noise or transient spikes that may trigger a false alarm if only a single frequency sideband was monitored. Furthermore, as we have shown in the paper, some of the wide-band signals such as Irq show a significant increase in their fault magnitudes and the most consistency across the wide-band frequencies monitored. In addition, these signals may be able to be used to detect an incipient fault earlier than other less sensitive signals. These benefits can help to minimize the potential damage that could occur if a fault continued and lead to a failure. Therefore, by potentially minimizing more severe damage occurring to equipment and the resultant unintended downtime is of significant benefit and increase reliability.

The presented wide-band results emphasize that if also utilized in a data fusion approach with the sideband signals, there is a much greater chance of a positive fault alarm signal, which illustrates how the controller signals (especially Irq) can be used in combination with other signals to potentially build a more robust and reliable fault detection and conditioning monitoring system for electric machines. The benefits of this, particularly for offshore WTs, are important such as maintaining turbine operation and continuing to produce electricity and hence, minimizing cost impact on the electricity generated making it more profitable for the operator and cheaper for the consumer.

VII. Conclusion

This paper reported on a novel investigation of the wide-band spectral signatures in the controller signals of DFIGs, with a view to characterizing them for rotor electrical fault detection. A set of analytical equations was first presented, which can calculate the wide-band frequency components in the spectra of the controller signals with and without REA. These equations were verified with a DFIG harmonic model in Matlab SIMULINK and also validated by experimental studies conducted on a purpose built laboratory DFIG test-rig.

It was found that a number of the wide-band, higher order, REA related frequency components can be identified in the spectra of the DFIG controller outer and inner loop signals. These reported REA related frequency components were shown to be sensitive to the existance of REA. Furthermore, the REA sensitivity of one of the inner loop controller signals (Irq) was shown to consistently have the highest magnitude in compared to the other controller signals across all the measured REA related sideband frequencies and, therefore, has considerable potential for fault detection.

The reported study of the REA related spectral signatures could be utilised for the development of improved controller embedded fault detection techniques.

Appendix A

The stator voltages and currents of a DFIG operating with REA (under the assumptions stated in Section II) are [31]:

$$\mathrm{V_{sx}(t)} = \mathrm{V_M}\cos(\omega t + \varphi_{vx}) \tag{A1}$$

$$\mathrm{I_{sx}(t)} = \sum_k \mathrm{I^k_{sM}}\cos([(1 \mp 2s) - 6k(1-s)]\,\omega t + \varphi_{Ix}) \tag{A2}$$

where: x denotes phase ($x = a$, b and c); φ_{vx} is 0, $2\pi/3$ and $4\pi/3$, respectively; and, φ_{Ix} is the power factor angle.

The stator active power, Ps, is:

$$\mathrm{P_s(t)} = \mathrm{V_{sa}I_{sa}} + \mathrm{V_{sb}I_{sb}} + \mathrm{V_{sc}I_{sc}} \tag{A3}$$

Substituting (A1) and (A2) into (A3), yields the following resultant stator active power equation:

$$\mathrm{P}_s(t) = 3/2\sum_k \mathrm{V_M I^k_M}\cos(2s - [6k(1-s)]\omega t) \tag{A4}$$

The stator reactive power, Qs, is:

$$\mathrm{Q_s(t)} = \frac{1}{\sqrt{3}}[(\mathrm{V_{sb}} - \mathrm{V_{sc}})\,\mathrm{I_{sa}} + (\mathrm{V_{sc}} - \mathrm{V_{sa}})\,\mathrm{I_{sb}} + (\mathrm{V_{sa}} - \mathrm{V_{sb}})\,\mathrm{I_{sc}}] \tag{A5}$$

Substituting (A1) and (A2) into (A5), yields the following resultant stator reactive power equation:

$$\mathrm{Q_s(t)} = 3/2 \sum_k \mathrm{V_M I_M^k} \cos(2s - [6k(1-s)]\omega t) \qquad \text{(A6)}$$

APPENDIX B

REA produces reverse sequence frequency components at all frequencies existing in the healthy rotor currents spectra, which can be calculated as [31]:

$$\mathrm{I_{rx}(t)} = \sum_k \mathrm{I_{rM}^k} \cos(\mp [s \mp 6k(1-s)]\, \omega t + \varphi_{Irx}) \qquad \text{(A7)}$$

The three-phase rotor currents (given in (A7)) are converted into the synchronously rotating reference frame by applying a slip angle, θ_{slip}, to a standard Park transformation. As a result, the rotor currents in the synchronously rotating reference frame are:

$$\mathrm{I_{rdq}(t)} = \sqrt{3/2} \sum_k \mathrm{I_{rM}^k} \cos(2s - [6k(1-s)]\omega t) \qquad \text{(A8)}$$

REFERENCES

[1] S. Asadollash, R. Zhu, and M. Liserre, "Analysis of voltage control strategies for wind farms," *IEEE Trans. Sustain. Energy*, vol. 11, no. 2, pp. 1002–1012, Apr. 2020.

[2] Y. Wang, X. Ma, and P. Qian, "Wind turbine fault detection and identification through PCA-based optimal variable selection," *IEEE Trans. Sustain. Energy*, vol. 9, no. 4, pp. 1627–1635, Oct. 2018.

[3] C. J. Crabtree, D. Zappalá, and P. J. Tavner, "Survey of commercially available condition monitoring systems for wind turbines," Durham Univ. School Eng. Comput. Sci. and the SUPERGEN Wind Energy Technologies Consortium, Techn. Rep., 2014.

[4] W. Qiao and D. Lu, "Survey on wind turbine condition monitoring and fault diagnosis-Part i: Components and subsystems," *IEEE Trans. Ind. Electron.*, vol. 62, no. 10, pp. 6536–6545, Oct. 2015.

[5] Y. Lin *et al.*, "Fault analysis of wind turbines in China," *Renew. Sustain. Energy Rev.*, vol. 55, pp. 482–490, 2016.

[6] J. Carroll, A. McDonald, and D. McMillan, "Failure rate, repair time and unscheduled o&m cost," *Wind Energy*, vol. 19, p. 1107–1119, 2015.

[7] M. Edrah, K. L. Lo, and O. Anaya-Lara, "Impacts of high penetration of dfig wind turbines on rotor angle stability of power systems," *IEEE Trans. Sustain. Energy*, vol. 6, no. 3, pp. 759–766, Jul. 2015.

[8] L. G. Meegahapola, T. Littler, and D. Flynn, "Decoupled DFIG fault ride-through strategy for enhanced stability performance during grid faults," *IEEE Trans. Sustain. Energy*, vol. 1, no. 3, pp. 152–162, Oct. 2010.

[9] M. Zaggout, P. Tavner, C. Crabtree, and L. Ran, "Detection of rotor electrical asymmetry in wind turbine doubly-fed induction generators," *IET Renew. Power Gener.*, vol. 8, no. 8, pp. 878–886, Nov. 2014.

[10] M. B. Abadi *et al.*, "Inter-turn fault detection in doubly-fed induction generators for wind turbine applications using the stator reactive power analysis," in *Proc. Renew. Power Gener. Conf.*, 2014, pp. 1–6.

[11] A. Stefani, A. Yazidi, C. Rossi, F. Filippetti, D. Casadei, and G. Capolino, "Doubly fed induction machines diagnosis based on signature analysis of rotor modulating signals," *IEEE Trans. Ind. Appl.*, vol. 44, no. 6, pp. 1711–1721, Nov./Dec. 2008.

[12] W. Qiao and D. Lu, "A survey on wind turbine condition monitoring and fault diagnosis—Part II: Signals and signal processing methods," *IEEE Trans. Ind. Electron.*, vol. 62, no. 10, pp. 6546–6557, Oct. 2015.

[13] W. Qiao, P. Zhang, and M. Chow, "Condition monitoring, diagnosis, prognosis, and health management for wind energy conversion systems," *IEEE Trans. Ind. Electron.*, vol. 62, no. 10, pp. 6533–6535, Oct. 2015.

[14] Z. Yang and Y. Chai, "A survey of fault diagnosis for onshore grid-connected converter in wind energy conversion systems," *Renew. Sustain. Energy Rev.*, vol. 66, pp. 345–359, 2016.

[15] M. Riera-Guasp, J. A. Antonino-Daviu, and G. Capolino, "Advances in electrical machine, power electronic, and drive condition monitoring and fault detection: State of the art," *IEEE Trans. Ind. Electon.*, vol. 62, no. 3, pp. 1746–1759, Mar. 2015.

[16] A. Bellini, F. Flippetti, G. Franceschini, and C. Tassoni, "Closed-loop control impact on the diagnosis of induction motors faults," *IEEE Trans. Ind. Appl.*, vol. 36, no. 5, pp. 1318–1329, Sep./Oct. 2000.

[17] S. A. Saleh and E. Ozkop, "Phaselet-based method for detecting electric faults in 3φ induction motor drives-part ii: performance evaluation," *IEEE Trans. Ind. Appl.*, vol. 53, no. 3, pp. 2988–2996, May/Jun. 2017.

[18] Y. Gritli, L. Zarri, C. Rossi, F. Filippetti, G. Capolino, and D. Casadei, "Advanced diagnosis of electrical faults in wound-rotor induction machines," *IEEE Trans. Ind. Electron.*, vol. 60, no. 9, pp. 4012–4024, Sep. 2013.

[19] L. Zarri, Y. Gritli, C. Rossi, and F. Filippetti, "Fault detection based on closed-loop signals for induction machines," in *Proc. IEEE Workshop Elect. Mach. Des. , Control Diagnosis*, 2015, pp. 261–270.

[20] S. M. A. Cruz and A. J. M. Cardoso, "Fault indicators for the diagnosis of rotor faults in foc induction motor drives," in *Proc. IEEE Int. Electric Mach. Drives Conf.*, 2007, pp. 1136–1141.

[21] D. Casadei *et al.*, "Closed loop bandwidth impact on doubly fed induction machine asymmetries detection based on rotor voltage signature analysis," in *Proc. 43rd Int. Univ. Power Eng. Conf.*, 2008, pp. 1–5.

[22] J. Faiz and S. M. M. Moosavi, "Detection of mixed eccentricity fault in doubly-fed induction generator based on reactive power spectrum," *IET Electric Power Appl.*, vol. 11, no. 6, pp. 1076–1084, 2017.

[23] D. Shah, S. Nandi, and P. Neti, "Stator-interturn-fault detection of doubly fed induction generators using rotor-current and search-coil-voltage signature analysis," *IEEE Trans. Ind. Appl.*, vol. 45, no. 5, pp. 1831–1842, Sep./Oct. 2009.

[24] S. Djurovic, C. J. Crabtree, P. J. Tavner, and A. C. Smith, "Condition monitoring of wind turbine induction generators with rotor electrical asymmetry," *IET Renew. Power Gener.*, vol. 6, no. 4, pp. 207–216, Jul. 2012.

[25] E. Artigao, A. Honrubia-Escribano, and E. Gomez-Lazaro, "Current signature analysis to monitor DFIG wind turbine generators: A case study," *Renew. Energy*, vol. 116, no. B, pp. 5–14, 2018.

[26] M. E. H. Benbouzid and G. B. Kliman, "What stator current processing-based technique to use for induction motor rotor faults diagnosis?" *IEEE Trans. Energy Convers.*, vol. 18, no. 2, pp. 238–244, Jun. 2003.

[27] D. Zappalá *et al.*, "Side-band algorithm for automatic wind turbine gearbox fault detection and diagnosis," *IET Renew. Power Gener.*, vol. 8, no. 4, pp. 380–389, 2013.

[28] N. Sarma, P. M. Tuohy, and S. Djurovic, "Modeling, analysis and validation of controller signal interharmonic effects in DFIG drives," *IEEE Trans. Sustain. Energy*, vol. 11, no. 2, pp. 713–725, Apr. 2020.

[29] N. Sarma *et al.*, "DFIG stator flux oriented control scheme execution for test facilities utilising commercial converters," *IET Renew. Power Gener. J.*, vol. 12, no. 12, pp. 1366–1374, 2018.

[30] S. Djurović, D. S. Vilchis-Rodriguez, and A. C. Smith, "Supply induced interharmonic effects in wound rotor and doubly-fed induction generators," *IEEE Trans. Energy Convers.*, vol. 30, no. 4, pp. 1397–1408, Dec. 2015.

[31] S. Williamson and S. Djurovic, "Origins of stator current spectra in dfigs with winding faults and excitation asymmetries," in *Proc. IEEE Int. Electric Mach. Drives Conf.*, Miami, FL, USA, 2009, pp. 563–570.

[32] D. Zappalá *et al.*, "Electrical & mechanical diagnostic indicators of wind turbine induction generator rotor faults," *Renew. Energy*, vol. 131, pp. 14–24, 2019.

[33] N. Sarma, K. Tshiloz, D. S. Vilchis-Rodriguez, and S. Djurović, "Modelling of induction machine time and space harmonic effects in the simulink environment," in *Proc. IEEE Int. Electric Mach. Drives Conf.*, 2015, pp. 1279–1285.

[34] Y. Gritli *et al.*, "Experimental validation of doubly fed induction machine rotor fault diagnosis based on wavelet analysis in closed-loop operations," in *Proc. Int. Symp. Power Electron., Elect. Drives, Autom. Motion*, 2010, pp. 513–518.

[35] N. Sarma, J. M. Apsley, and S. Djurovic, "Implementation of a conventional dfig stator flux oriented control scheme using industrial converters," in *Proc. IEEE Int. Conf. Renew. Energy Res. Appl.*, Birmingham, U.K., 2016, pp. 236–241.

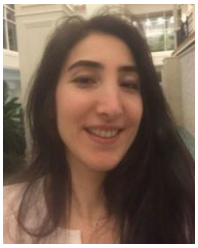

Nur Sarma (Member, IEEE) received the B.Sc. and MSc degrees in electrical and electronic engineering (EEE) from Sakarya University, Turkey. She subsequently received her Ph.D. degree in EEE from The University of Manchester, UK, in 2017. She is currently working in Düzce University, Turkey, as an Assistant Professor. Her research interests are in fault diagnosis and condition monitoring of electric machines, renewable power generation and power conversion.

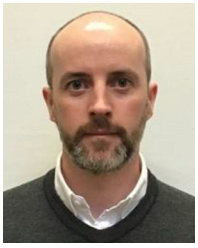

Paul M. Tuohy received the B.Eng. (Hons.) degree in mechatronics with industrial experience and the Ph.D. degree in electrical engineering from The University of Manchester, Manchester, UK, in 2006 and 2011, respectfully, He is currently a Research Fellow at the Rolls-Royce University Technology Centre (Electrical Systems for Extreme Environments) at The University of Manchester, Manchester, UK. His research interests include the design, finite element analysis, and testing of electric machines, actuators and drives for aerospace, vehicle, marine and renewable energy applications. Dr. Tuohy was the recipient of the Siemens Medal in 2006. He was elected Whitworth Scholar in 2007 and Whitworth Senior Scholar in 2012. He is also the holder of two patents.

Anees Mohammed received the M.Sc. degree in electrical power engineering from University of Newcastle, UK, in 2010 and the Ph.D. degree in electrical and electronic engineering at the University of Manchester, UK in 2019. He worked as a Research Associate with the Power Conversion Group at University of Manchester and spent four years working as Assistant Lecturer at Benghazi University, Libya. He currently works for Dyson, UK. His research interests are in electric machines, drives and condition monitoring.

Siniša Djurović (Member, IEEE) received the Dipl. Ing. degree in electrical engineering from the University of Montenegro in 2002 and the Ph.D. degree from the University of Manchester in 2007. He is currently a Senior Lecturer with the Power Conversion Group at Manchester. His research interests are in the area of operation, design, monitoring and diagnostics of electric machines and drives.